Analytical Methods

Accepted Manuscript

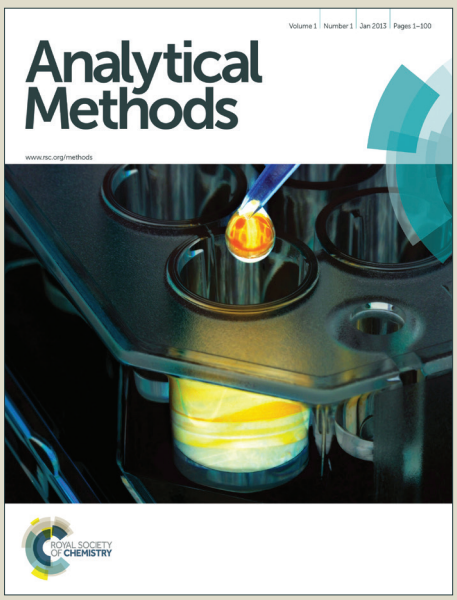

ROYAL SOCIETY OF CHEMISTRY

www.rsc.org/methods

Reduced graphene oxide/α-cyclodextrin hybrid for detection of methionine: electrochemical, fluorometric and computational study

Erhan Zor[1,2], *Muhammed Esad Saglam*[3], *Sabri Alpaydin*[3], *Haluk Bingol*[3]*

[1]Science Institute, Selcuk University, Konya, Turkey

[2]Science and Technology Department, A. K. Education Faculty, Necmettin Erbakan University, Konya, Turkey

[3]Department of Chemistry, A. K. Education Faculty, Necmettin Erbakan University, Konya, Turkey

zorerhan@gmail.com, muhammedesadsaglam@gmail.com, sabrialp@gmail.com, halukbingol@gmail.com

[*]***Corresponding author****:* Haluk Bingol - email: halukbingol@gmail.com, tel. +903323238220 - 5499, fax: +903323238225

Abstract

We report on fluorometric and voltammetric detection of *L*-methionine (*Met*) based on host–guest interaction between *Met* and reduced graphene oxide/*α*-cyclodextrin (*rGO/α-CD*) hybrid material. For voltammetric measurements, *rGO/α-CD* was used as electrode modification material and the successful detection of *Met* was achieved. Also, *rGO/α-CD* was used as a fluorescence quencher (turn off) for luminol which was employed as a fluorescence probe. The addition of *Met* into the same solution gave rise to fluorescence enhancing (turn on) after the host–guest recognition between *Met* and *rGO/α-CD* which caused the release of luminol. The interactions of luminol and *Met* with *rGO/α-CD* were modeled by molecular docking using AutoDock Vina and the interaction energies were predicted as –4.3 and –4.4 kcal mol^{-1}, respectively. The proposed biosensor is considered to be a promising model for detection of *Met*.

Keywords: Reduced graphene oxide; *α*-cyclodextrin; methionine; luminol; fluorometric sensor; electrochemical biosensor; molecular docking.

1.Introduction

Molecular recognition is one of the most fundamental properties of various systems in supramolecular chemistry including non-covalent interactions of molecular receptors with a target analyte to build multicomponent assemblies.[1,2] The design and building of receptors, which exhibit high affinity and high selectivity, have received considerable attention and have been central to various biological and supramolecular assemblies in recent years.[3,4,5] The sophistication of supramolecular receptors covers the selective determination of bio-organic molecules which enable and support life functions in living systems. Among amino acids, for instance, *L*-methionine (*Met*) is an essential amino acid and plays a fundamental role as a precursor of various amino acids such as cysteine, taurine, glutathione and polyamines.[6] *Met* is the major source of methyl groups for formation of DNA, RNA and other molecules.[7] Moreover, *Met* is a source of sulphur in the diet, prevents the disorders in hair and skin, also it helps to reduce cholesterol levels by increasing the lecithin production in liver.[8] The deficiencies of *Met* might manifest many important diseases such as toxemia, muscle paralysis, hair loss, depression, liver deterioration, impaired growth, Parkinson's disease and AIDS which stems from HIV infection.[9] Considering the significant importance of *Met*, the sensitive determination of *Met* level is very important in the clinical point of view.

Various techniques, such as flow injection-amperometric detection,[10] high-performance liquid chromatography,[11] capillary electrophoresis [12] and chemiluminescence,[13] have been developed for determination of *Met*. Although the reported techniques are useful for the determination of *Met*, many of them have several disadvantages such as long analysis time and high cost. In this context, electrochemical methods have been one of the widely used methods for the determination of biological components owing to their advantages such as ease of preparation, practical application, low material cost, accuracy, high sensitivity and stability.[14] Fluorescence quenching-based turn-on assay is another approach, which is one of

the most important applications among the various fluorescence based techniques, in which the transfer of photo-excitation energy from a donor fluorophore to an acceptor molecule can be effectively quenched.[15,16] The quenched fluorescence can be ‘‘turned-on’’ upon the addition of target analytes, and the recovery of the fluorescence intensity can be calculated as proportional to the concentration of target analytes.[16]

In addition to these methods, the studies in a multidisciplinary approach including experimental studies combined with theoretical calculations have received accelerating attention, because theoretical approaches can provide rationalization of experimental observation as well as predictions relating the outcome of future experiments.[17,18] A theory consisting of molecular simulations at the atomic level (molecular modeling) is used to explain the molecular recognition of supramolecular receptor and it is called as "molecular docking". Molecular docking can provide an insight into the preferred binding location between acceptor and receptor molecules and can corroborate experimental results.[19,20]

Graphene is defined as a one-atom-thick planar sheet of sp^2-bonded carbon atoms which are arranged in a two-dimensional honeycomb lattice.[21,22,23] Usually, working with modified forms of graphene begins with graphene oxide (GO) on which tunable oxygenated functional groups such as hydroxyl, epoxide, carboxyl or ester moieties exist.[24,25] Due to the fact that GO can be readily functionalized with receptor units, graphene-based biosensors have been one of the fascinating applications in electrochemical sensing platform of biomolecules.[25] Also, in recent years, the "fluorescence turn-on" principle has shown significant advantages in bio-sensing applications of graphene based materials which can act as a highly efficient fluorescence quenchers. [26,27] Chang and co-workers showed that graphene is a good energy acceptor in energy transfer due to its peculiar electronic properties.[27] Both theoretically[29] and experimentally,[30] the fluorescence quenching effect of graphene was observed. In spite of being a disrupted lattice of sp^2-bonded carbon atoms, GO can display

similar behavior and it has been reported to be a highly efficient long-range fluorescence quencher.[31] Morales-Narváez and Merkoçi indicated that the oxygenated lattice of GO not only makes it water dispersible but also allows noncovalent interaction with amine functional groups, diols and phenyls groups in biomolecules through electrostatic interaction, π–π stacking, and hydrogen bonding which leads to recognize of biomolecules with high specificity.[31] In addition, the functionalization of graphene oxide can increase the quenching performance with extraordinary selective interaction of target analyte.

Herein, we report the design, fabrication and performance of a novel electrochemical and fluorometric biosensor. In the electrochemical measurements, *rGO/α-CD* functionalized GCE was used as biosensor. For fluorometric studies, *rGO/α-CD* was used as fluorescence quencher for luminol which was employed as fluorescence probe (based on its quenching performance). The interaction between luminol/*Met* and *rGO/α-CD* was investigated by molecular docking due to the fact that it is a useful tool to confirm the binding mode, and the interaction energy between ligand and receptor was evaluated.

2. Experimental

2.1. Chemicals and equipment

All commercial reagents were of analytical grade and handled according to the material safety data sheets suggested by the suppliers. Graphite powder (99.99%), concentrated H_3PO_4 and H_2SO_4, H_2O_2 (30%), $KMnO_4$ (99%), P_2O_5, *α*-Cyclodextrin, luminol and *L*-methionine (*Met*) were purchased from Sigma-Aldrich. All aqueous solutions were freshly prepared in Milli-Q ultra-pure water.

Fourier transformed infrared (FT-IR) spectra of the samples were recorded between 550 and 4000 cm^{-1} using ATR FT-IR spectrometer (Perkin Elmer 100 FT-IR). Thermogravimetric analysis (TGA) of the samples (10–15 mg) was performed on Setaram

thermal gravimetric analyzer (France) at temperature range of 25–1200 ˚C with 10˚C min^{-1} heating ramp under argon atmosphere (gas flow rate: 20 mL min^{-1}). Electrode morphologies were investigated by scanning electron microscopy (SEM), performed on a ZEISS EVO LS 10. Fluorescence measurements were carried out in a QuantaMaster™ 40 spectrofluorometer (QM40 PTI, Photon Technology International) combined with FelixGX spectroscopy software. Electrochemical measurements were performed with an IVIUM-CompactStat potentiostat (Ivium Technologies, Netherlands) combined with a BAS/C3 electrochemical cell stand using three electrode configuration cell. GCE, Ag/AgCl electrode (with luggin tip) and platinum electrode were used as the working electrode, reference electrode and counter electrode, respectively. *Sonorex* Super RK 106 (Germany) was used as ultrasonic bath. All experiments were performed in 0.10 M sodium acetate and sodium phosphate buffer solution (A-PBS) at pH 7.40.

2.2. The synthesis of α-Cyclodextrin Functionalized Graphene (*rGO/α-CD hybrid*)

Graphene oxide (GO) was synthesized from graphite powder according to the improved method[32] with an additional preoxidation process, which has significant advantages, such as the applied method yields a higher fraction of well-oxidized hydrophilic carbon material, does not generate toxic gas and the temperature can be easily controlled, over Hummers' method.[33] Briefly; 3.0 g graphite powder was pre-oxidized in a mixture of 15 mL concentrated H_2SO_4, 1.5 g $K_2S_2O_8$ and 1.5 g P_2O_5. The mixture was then diluted with ultra-pure water, filtered and dried in vacuum oven at 50 ˚C. After that, the preoxidized graphite was re-oxidized by improved method in a 9:1 mixture of concentrated H_2SO_4/H_3PO_4 (360:40 mL) containing $KMnO_4$ (18.0 g) for producing of GO. Then, *α*-cyclodextrin (*α-CD)* functionalized graphene was synthesized as indicated literature as follows[34]: A 10.0 mL graphene oxide solution (0.5 mg mL^{-1}) was sonicated 30 min to obtain a homogeneous dispersion. Then, it was mixed with 10.0 mL of 40 mg *α-CD* aqueous solution and 150.0 μL

of ammonia solution, followed by the addition of 10 µL of hydrazine solution. After shaken a few minutes, the solution was immersed in a water bath (60 °C) for 3.5 h to obtain a stable black dispersion. The dispersion was filtered to obtain *rGO/α-CD* hybrid which can be re-dispersed readily in water by ultrasonication.

2.3. Procedure for voltammetric and fluorometric experiments

Cyclic voltammetry measurements were carried out in A-PBS buffer (pH 7.40, as an optimum condition) with 0.10 M KCl at ambient temperature (at 25°C). For modification process of hybrid material, GCE surfaces were firstly polished with 1.0, 0.3 and 0.05 µm alumina slurry on a felt pad, and washed with ultra-pure water. The GCE was then immersed in water and methanol for 15 minutes, respectively in order to remove residual alumina particles by sonication in an ultrasonic bath. The electrode was dried at room temperature before the modification step. After drying, the *rGO/α-CD/GCE* was prepared by casting 5.0 µL of *rGO/α-CD* (0.2 mg mL^{-1}) suspension. Finally, the obtained electrode was dried at room temperature overnight. The *rGO/α-CD/GCE* was then washed with ultra-pure water and dried before the use. SEM images of the bare GCE and *rGO/α-CD/GCE* were given in Fig. S1 (Supporting Information).

In fluorometric measurements, luminol was used as fluorometric probe and the stock solution was freshly prepared as 2.0×10^{-3} M with mixed solution of 0.10 M A-PBS buffer solution at pH 7.40. The working solution of luminol was 2.0×10^{-7} M for all experiments. The stock solution of *rGO/α-CD* hybrid was prepared as 1 mg mL^{-1} in A-PBS buffer solution at pH 7.40 and was sonicated 30 min prior to use. All solutions were stored at +4 °C in a brown flask. The fluorometric intensity was measured in the wavelength range of 360–540 nm upon excitation at 300 nm in stoppered cuvet. To achieve stable results, the fluorometric measurements were performed after waiting around 5 min.

2.4. Procedure for simulation method - molecular docking study

AutoDock Vina (ADVina) has been one of the widely used simulation programs in molecular docking studies because it displays good free energy correlation values between docking simulations and experimental data.[35,36] Due to this, ADVina program was employed for docking studies considering the algorithm which maintains a rigid macromolecule while allowing ligand flexibility.[37]

The crystal structure of α-CD was taken from the protein data bank (PDB code 1CXF). All the hydrogen bonds for each rim of α-CD were oriented in the same direction.[38] The two-dimensional (2D) structures of the luminol, *Met*, GO and rGO were drawn using ChemBioDraw v13.0. The starting geometries of four different structures of GO and the structure of rGO (edges of rGO were modified to contain both carboxyl and hydroxyl groups) were constructed considering the previous related literature.[39,40,41] After the 2D sketches were converted into three dimensional (3D) images and the structures were energetically minimized, new coordinates were updated and recorded in PDB format using Discovery Studio v3.5. The constructed graphene derivatives were assumed to be pristine and defect-, lesion-, and grain boundary-free. Before starting the molecular docking, the AutoDockTools version 1.5.6 (ADT) was used to optimize the guest compounds from the PDB files as adding Gasteiger charges, assigning polar hydrogen atoms and setting up rotatable bonds. The pdbqt format files (required as input ADVina) were generated using ADT. The docking procedure was carried out in two parts: Part 1; α-CD was docked to rGO using the following cartesian coordinates: x=0 Å, y=0 Å, z=0 Å. A docking grid with a dimension of 60 Å×70 Å×40 Å and a grid spacing of 1.000 Å was applied. Part 2; taking into account the docking conformation results of part 1, luminol and *Met* were docked to *rGO/αCD* combination using the following cartesian coordinates: x=–1.300 Å, y=–1.500 Å, z=–11.600 Å. A docking grid with a dimension of 12 Å×12 Å×24 Å and a grid spacing of 1.000 Å was applied. All the other

parameters were used as defined by ADVina for each docking steps. The resulting 9 binding models were further analyzed to find the most suitable binding model in each case. The preferred binding model having the minimum energy with the maximum number of poses clustered in that site was selected.[41] The ADVina output results were represented the docking scores as free energy change (ΔG_{bind}) of binding and were further converted to the predicted binding constants (K_{bind}) using $K_{bind}=exp(\Delta G_{bind}/RT)$ at 25°C.

All experimental procedure explained above was collected in Scheme 1.

Here Scheme 1

3. Results and discussion

3.1. Characterization of the rGO/α-CD hybrid material

FT-IR spectral analysis was performed to confirm the presence of *rGO/α-CD* structure. The comparable changes in the spectral features of GO and *α*-CD can be seen in Fig. 1A (also plotted on separate axes in Fig. S2, Supporting Information). All spectra have characteristic broad bands in the range of 3040–3580 cm^{-1} for O–H stretching vibration in the range of 2880–2980 cm^{-1} asymmetric stretching and symmetric vibrations of CH_2.[34,42] The spectrum of GO also shows the characteristic stretching vibrational modes at 1731, 1633, 1221 and 1059 cm^{-1} attributed to C=O (carbonyl), C=C (aromatic), C–O (epoxy) and C–O (alkoxy) situated on the GO sheet, respectively.[42,43] After the reduction of GO to rGO sheet, the peak intensity at 1731 cm^{-1} was greatly disappeared for rGO and *rGO/α-CD*, while the peaks of other oxygen-containing functional groups were weakened through the reduction process, indicating that most of the oxygen-containing functional groups were removed from GO.[44] Also, rGO and *rGO/α-CD* shows the remained characteristic C=C (aromatic) vibrational modes at 1670 and 1665 cm^{-1}, respectively. These observations show that GO

have been successfully reduced to rGO (or *rGO/α-CD*). In addition, in the spectrum of *rGO/α-CD*, the presence of characteristic *α*-CD absorption bands[45] at 1587, 1147 and 1013 cm^{-1} clearly confirms that *α*-CD molecules are settled on rGO sheet. When *rGO/α-CD* was formed, the broad vibration peak of O–H stretching for *α*-CD at around 3298 cm^{-1} exhibited slightly disruption and red-shift to lower wave number in the spectrum of *rGO/α-CD*. This situation can be described by a strong hydrogen bond between *α*-CD molecules and some oxygen-containing groups of rGO moiety[46,47] and it also effectively decreases the bond energy and the broad vibrational peak shows red-shift (to lower energy). As a result, it can be concluded that the phenomena of the chemically synthesized *rGO/α-CD* result from the presence of hydrogen bonding between the doping graphene oxide sheets and *α*-CD backbone as emphasized by Guo et al.[34]

Here Figure 1

The thermal stability and the composition of the prepared *rGO/α-CD* were examined and compared with that of GO, rGO and *α*-CD using TGA. As shown in Fig. 1B, all components exhibited a mass loss (4.38wt% for GO, 8.72wt% for rGO, 8.72wt% for *α*-CD and 4.27wt% for *rGO/α-CD*) below 120 °C due to evaporation of water molecules held in the samples.[48] GO is thermally unstable and shows the characteristic major mass loss (64.6wt%) appeared between 145 and 220 °C which was attributed to the decomposition of some oxygen-containing functional groups, such as –COOH, –OH, –O–, etc. yielding carbon monoxide, carbon dioxide and water vapor as similarly indicated in the earlier reports.[39,49] On the contrary, rGO displays better thermal stability and its slight mass loss (2.6wt%) in this range indicates that the oxygen-containing functional groups are largely removed by hydrazine hydrate during the reduction process. Compared to rGO, in the range of 230–400 °C, *rGO/α-CD* displays a subsequent decrease in mass loss (58.1 wt%) attributed to the decomposition of *α*-CD moiety adsorbed on rGO, which is in accordance with the thermal

decomposition of α-CD given in same figure. These results verify that α-CD molecules would be located on the surface of rGO.

3.2. Electrochemical measurement results

Fig. 2A shows the cyclic voltammograms obtained at *rGO/α-CD/GCE* in the absence and presence of *Met* (2.0×10^{-3} M) in 0.10 M A-PBS (pH 7.40) at the scan rate of 50 mV s^{-1}. Similar to the previous study,[50] an irreversible anodic peak was observed at 1.28 V with GCE (the inset of Fig. 2A). As reported by Jeevagan and John,[9] this peak was not stable after five cycles and they suggest that the bare GCE cannot be used for the stable and accurate determination of *Met*. On the other hand, *rGO/α-CD/GCE* displayed a well-defined irreversible anodic peak at 1.46 V in the presence of *Met*. This peak was highly stable even after keeping the modified electrode in buffer solution for 7 days indicating that *rGO/α-CD/GCE* can be used for the stable and accurate determination of *Met*. The obtained clear voltammetric signal with higher oxidation current value for *Met* at *rGO/α-CD/GCE* can be attributed to (1) the interaction of *Met* with α-CD and (2) the electrocatalytic activity of rGO (due to the large surface area which could allow rapid heterogeneous electron transfer) significantly increased the catalytic activity.[51]

Here Figure 2

Fig. 2B shows the cyclic voltammograms for the oxidation process of *Met* at different scan rates. As can be easily seen in the inset of Fig. 2B, the plot of the oxidation peak current versus the square root of the scan rate ($v^{1/2}$) displays a straight line at scan rate ranging 25–300 mVs^{-1}, as expected for a diffusion-limited electrochemical process. Moreover, as a result of the electrochemical irreversible processes, the peak current increased with an increase at the scan rate and the peak shifted toward more positive potential values.[52]

Here Figure 3

In order to investigate the amperometric response of *rGO/α-CD/GCE* versus *Met* at lower concentration, CA technique was performed by successive addition of 1.7×10^{-4} M–1.2×10^{-3} M *Met* to a continuously stirred 0.10 M A-PBS solution at 0.00 and 1.46 V *vs.* Ag/AgCl (3 M KCl) and results were shown in Fig. 3. When an aliquot of *Met* was dropped into the stirring A-PBS solution, the oxidation current value steeply rose to reach a stable value. As it can be easily seen, *rGO/α-CD/GCE* exhibited an excellent amperometric response to the increasing concentration of *Met* with ΔI_{max} of 30 μA. As presented in the inset of Fig. 3, the amperometric results displayed that the oxidation peak current of *Met* linearly increases with the increasing concentration of *Met* in the range of 1.7×10^{-4} M–1.2×10^{-3} M. Considering the equation of the linear regression of calibration graph, the limit of detection (LOD) and the limit of quantitation (LOQ) values were calculated as 4.0×10^{-5} M and 1.20×10^{-4} M, respectively, by the standard deviation of y–intercept and the slope of the regression line.

3.3. Fluorometric measurement results

In order to confirm and deeply examine the interactions between *Met* and *rGO/α-CD* in aqueous media, luminol was used as a fluorescence probe based on its fluorescence properties quenched with *rGO/α-CD*.

Here Figure 4

Fig. 4A shows the emission spectra of luminol in the presence of different concentration of *rGO/α-CD*. The emission spectra of luminol decreased and almost quenched by the addition of the specified amounts of *rGO/α-CD* when interacted with *rGO/α-CD*. The fluorescence intensity of luminol quenched nearly 90% by *rGO/α-CD* of 500 μg mL^{-1}. In this point, it is also important to note that no (or negligibly small) quenching effect was observed

in the presence of GO, rGO and bare *α*-CD under the same conditions. This situation can only be explained by the interaction of luminol with *α*-CD moiety on rGO sheet. For more detailed evaluation of the quenching properties of luminol caused by *rGO/α-CD*, the classical Stern–Volmer equation[53] was used. As can be seen in Fig. 4B, the obtained Stern–Volmer plot of F_0/F against the amount of *rGO/α-CD* showed an upward curvature. This kind of deviation from linear plot indicates the simultaneous presence of two types of fluorescence quenching; the dynamic quenching and static quenching.[53,54] Whereas the dynamic quenching stems from the dynamic collisions, the static quenching arises from the possibility of the formation of ground state complexes between luminol and *rGO/α-CD*, which agrees with our discussion above. Similar mixed quenching properties of graphene derivatives were observed for different fluorescent molecules, such as aminopyrene,[55] rhodamine 6G,[56] porphyrins.[57]

In the further step of the fluorescence study, the recognition of *Met* to *rGO/α-CD* was examined by reversible binding experiment. Whereas the presence of *rGO/α-CD* quenched the fluorescence of luminol, the addition of *Met* to the same solution resulted in an increase of the fluorescence intensity with the increasing concentration of *Met* from 1.7×10^{-3} M to 1.0×10^{-2} M as shown in Fig. 5A. This result can be attributed to the formation of strong *Met-rGO/α-CD* complex upon the addition of *Met* which actually makes luminol inaccessible and thus, luminol remains free from *rGO/α-CD*. It can be clearly seen in Fig. 5B, a good linear relationship is obtained between the fluorescence intensity and the concentration of *Met* in the concentration range of 1.7×10^{-3} M to 1.0×10^{-2} M (R^2=0.9801).

Here Figure 5

3.4. Molecular docking results

Due to the molecular docking technique is an attractive scaffold for host-guest chemistry, mainly in a non-covalent fashion, the computational docking studies were performed by placing a small molecule into the binding site of the target-specific region of the receptor. The studies were carried out to predict the binding energies of the complexes occurring between luminol (or *Met*) and *rGO/α-CD* by employing ADVina.

Here Figure 6

Due to the need of the explanation for the interaction between *α*-CD and GO as stated by Guo et. al that the detailed interaction mechanism between graphene sheets and CDs is not very clear and needs further study,[34] in the first part of the docking process, computational studies were employed to show the interaction of *α*-CD with GO. As shown in Fig. 6A, *α*-CD preferentially settled on the basal plane rather than the edges for the constructed four different structures of GO in each case. *α*-CD would be adsorbed on the surface of GO owing to the strong hydrogen bonding and also electrostatic forces and hydrophobic interactions[58], which is in accordance with the above IR data and molecular docking results. It is also important to note that the edges of GO failed to provide sufficient surface area for stabilization of the interactions between *α*-CD and GO as depicted in the previous literature.[41] On the other hand, the performed molecular docking studies showed that *α*-CD attaches on GO from the wide rim. The binding from wide rim of *α*-CD to hydrophilic surface of GO can be explained by the fact that the wide rim of the torus is distinctly hydrophilic while the narrow rim bearing the primary hydroxyl groups is intensely hydrophobic for CDs.[17] Among the nine possible interaction models calculated by ADVina, the overall binding energy of *α*-CD to GO was predicted as –8.9 kcal mol^{-1} for the most suitable interaction at which *α*-CD attaches on GO

from the wide rim. Afterwards, the rest of oxygen-containing groups on *GO/α-CD* skeleton surface would be reduced to produce *rGO/α-CD* (Fig. 6B) by strong reducing agent (hydrazine) as indicated in the literature.[34] The resultant structure of *rGO/α-CD* was used for the further molecular docking studies.

Here Figure 7

In the second part of the computational study, the docking models were evaluated for *rGO/α-CD*-luminol and *rGO/α-CD-Met* complexes. Fig. 7A and 7C show the docked models for *rGO/α-CD*-luminol in which luminol is surrounded by narrow rim, bearing the primary hydroxyl groups,[17] of *α*-CD attached on rGO. Unlike the interaction of luminol, *Met* penetrates into the cavity of *α*-CD as can be clearly seen in Fig. 7B and 7D. According to the docking results, the overall binding energies of luminol and *Met* to *rGO/α-CD* were predicted as –4.3 and –4.4 kcal mol^{-1}, respectively. The corresponding value of binding constants were calculated as 1.43×10^3 and 1.69×10^3 M^{-1}, respectively. Due to these close binding constant values, luminol can be replaced by *Met* when occurring simultaneously in the same solution which can be results in partly release of luminol as indicated in fluorometric measurements.

4. Conclusion

In this paper, a novel electrochemical and fluorometric sensor (*rGO/α-CD*) was developed for detection of *Met* in aqueous media. For the electrochemical experiment, the GCE surface was modified with *rGO/α-CD* and used as an electrochemical sensor. The results showed that the proposed sensor possesses an excellent electrocatalytic activity towards *Met* in a 0.10 M A-PBS solution at pH 7.40. In fluorometric measurements, luminol and *rGO/α-CD* were used as a fluorometric probe and fluorescence quencher, respectively. After the interaction of luminol with *rGO/α-CD*, the fluorescence intensity quenched. Luminol settled

on the narrow rim of the *α*-CD can be selectively replaced by *Met*. This result can be attributed to the close binding constant values of luminol and *Met* molecules. This replacement of luminol by *Met* released luminol in bulk solution with the resultant fluorescence "turn on" process. The addition of *Met* into the solution of luminol-*rGO/α-CD* increased the fluorescence of luminol which is directly related to the amount of *Met* added. Considering the fluorometric results, it is possible to realize that sensitive fluorescent sensing can be achieved using the functionalized graphene as fluorescence quencher. However, there are few reported studies on graphene based fluorescence amino acid sensors. It should be noted that the proposed electrochemical and fluorometric biosensor can be applied for the successful determination of *Met*. In the last part of the study, the molecular interactions were investigated by molecular docking in order to compare the experimental results with the computational results. The molecular docking results supported the voltammetric and fluorometric results indicating the interaction of *Met* with *rGO/α-CD* hybrid material. It can be concluded that this study is expected to be a promising platform for detection of target biomolecules by graphene based sensors using such different kind of methods.

Acknowledgments

The authors are grateful to the Scientific Research Projects of Necmettin Erbakan University (121210004/122010005) for financial support.

References

1 M. A. Jinks, H. Sun and C. A. Hunter, *Org. Biomol. Chem*., 2014, **12**, 1440–1447.

2 H. Bingol, E. Kocabas, E. Zor and A. Coskun, *Talanta*, 2010, **82**, 1538–1542.

3 H. Bingol, E. Kocabas, E. Zor and A. Coskun, *Electrochim. Acta*, 2011, **56**, 2057–2061.

4 M. Durmaz, S. Alpaydin, A. Sirit and M. Yilmaz, *Tetrahedron: Asymmetry*, 2007, **18**, 900–905.

5 M. Bayrakcı, A. N. Kursunlu, E. Güler and S. Ertul, *Dyes. Pigments*, 2013, **99**, 268–274.

6 M. Gómez-Mingot, J. Iniesta, V. Montiel, R. O. Kadara and C. E. Banks, *Sensor. Actuat. B-Chem*., 2011, **155**, 831–836.

7 A. F. Aissa, T. D. U. H. Gomes, M. R. Almeida, L. C. Hernandes, J. D. C. Darin, M. L. P. Bianchi and L. M. G. Antunes, *Food Chem. Toxicol*. 2013, **62**, 456–462.

8 B. B. Prasad, I. Pandey, A. Srivastava, D. Kumar and M. P. Tiwari, *Sensor. Actuat. B-Chem*., 2013, **176**, 863– 874.

9 A. J. Jeevagan and S. A. John, *Bioelectrochemistry*, 2012, **85**, 50–55.

10 J. A. Cox and E. D. Zlotorzynska, *Electroanalysis*, 1991, **3**, 239–242.

11 P. Houze, S. Gamra, I. Madelaine, B. Bousquet and B. Gourmel, *J. Clin. Lab. Anal*., 2001, **15**, 144–153.

12 A Zinellu, S. Sotgia, M. F. Usai, E. Zinellu, A. M. Posadino, L. Gaspa, R. Chessa, A. Pinna, F. Carta, L. Deiana and C. Carru, *Anal. Biochem.*, 2007, **363**, 91–96.

13 M. Hosseini, S. D. Abkenar, M. J. Chaichi, M. R. Ganjali and P. Norouzi, *Spectrochim. Acta A*, 2009, **72**, 484–489.

14 E. Zor, I. Hatay Patir, H. Bingol and M. Ersoz, *Biosens. Bioelectron*., 2013, **42**, 321–325.

15 C. Liu, Z. Wang, H. Jia and Zhengping Li, *Chem. Commun*., 2011, **47**, 4661–4663.

16 Y. Wang, S. Liu, Z. Liu, J. Yang and X. Hu, *J. Lumin*., 2014, **147**, 107–110.

17 K. B. Lipkowitz, *Chem. Rev*., 1998, **98**, 1829−1873.

18 X-H. Zhang, H-L. Wu, X-L. Yin, L-H. Li, J-Y. Wang, Y. Chen, C. Kang and R-Q. Yu, *Anal. Methods*, 2013, **5**, 710–717.

19 X. Li, G. Wang, D. Chen and Y. Lu, *RSC Adv.*, 2014, **4**, 7301–7312.

20 S. Vilar, G. Cozza and S. Moro, *Curr. Top. Med. Chem*., 2008, **8**, 1555–1572.

21 E. Morales-Narvaez, A-R. Hassan and Arben Merkoçi, *Angew. Chem. Int. Ed*. 2013, **52**, 13779–13783.

22 D. A. C. Brownson, S. A. Varey, F. Hussain, S. J. Haigh and C. E. Banks, *Nanoscale*, 2014, **6**, 1607–1621.

23 K. S. Novoselov, D. Jiang, F. Schedin, T. J. Booth, V. V. Khotkevich, S. V. Morozov and A. K. Geim, *Proc. Natl. Acad. Sci. U. S. A*., 2005, **102**, 10451–10453.

24 D. R. Dreyer, S. Park, C. W. Bielawski and R. S. Ruoff, *Chem. Soc. Rev.*, 2010, **39**, 228-240.

25 E. Zor, A. O. Saf, H. Bingol and M. Ersoz, *Anal. Biochem*., 2014, **449**, 83–89.

26 S. T. Huang, Y. Shi, N. Bing Li and H. Q. Luo, *Analyst*, 2012, **137**, 2593–2599.

27 X. Mao and H. Li, *J. Mater. Chem. B*, 2013, **1**, 4267–4272.

28 H. Chang, L. Tang, Y. Wang, J. Jiang and J. Li, *Anal. Chem*. 2010, **82**, 2341–2346.

29 R. S. Swathi and K. L. Sebastian, *J. Chem. Phys*., 2012, **130**, 233–240.

30 A. Kasry, A. A. Ardakani, G. S. Tulevski, B. Menges, M. Copel and L. Vyklicky, *J. Phys. Chem. C*, 2012, **116**, 2858−2862.

31 E. Morales-Narvez and A. Merkoçi, *Adv. Mater*., 2012, **24**, 3298–3308.

32 D. C. Marcano, D. V. Kosynkin, J. M. Berlin, A. Sinitskii, Z. Sun, A. Slesarev, L.B. Alemany, W. Lu and J. M. Tour, *ACS Nano*, 2010, **4**, 4806–4814.

33 W. S. Hummers and R. E. Offeman, *J. Am. Chem. Soc*. 1958, **80**, 1339–1339.

34 Y. Guo, S. Guo, J. Ren, Y. Zhai, S. Dong, and E. Wang, *ACS Nano*, 2010, **4**, 4001–4010.

35 X. Zhang, S. E. Wong, and F. C. Lightstone, *J. Comput. Chem*., 2013, **34**, 915–927.

36 J. Yan, G. Zhang, J. Pan and Y. Wang, *Int. J. Biol. Macromol*., 2014, **64**, 213–223.

37 O. Trott and A. J. Olson, *J. Comput. Chem*., 2010, **31**, 455–461.

38 J. Köhler and N. Grczelschak-Mick, *Beilstein J. Org. Chem*. 2013, **9**, 118–134.

39 S. Mao, H. Pu and J. Chen, *RSC Adv*., 2012, **2**, 2643–2662.

40 Y. Zhang , C. Wu , S. Guo and J. Zhang, *Nanotechnol. Rev*., 2013, **2**, 27–45.

41 G. P. Kotchey, B. L. Allen, H. Vedala, N. Yanamala, A. A. Kapralov, Y. Y. Tyurina, J. Klein-Seetharaman, V. E. Kagan and A. Star, *ACS Nano*, 2011, **5**, 2098-2108.

42 E. Zor, M. E. Saglam, I. Akin, A. O. Saf, H. Bingol and Mustafa Ersoz, *RSC Adv*.,2014, **4**,12457–12466.

43 N. A. Travlou, G. Z. Kyzas, N. K. Lazaridis and E. A. Deliyanni, *Langmuir*, 2013, **29**, 1657−1668.

44 V. Chandra and K. S. Kim, *Chem. Commun*., 2011, **47**, 3942–3944.

45 X. Shuai, F. E. Porbeni, M. Wei, I. D. Shin, and A. E. Tonelli, *Macromolecules*, 2001, **34**, 7355-7361.

46 D. S. Walker and G. L. Richmond, *J. Phys. Chem. C*, 2007, **111**, 8321–8330.

47 J. Joseph and E. D. Jemmis, *J. Am. Chem. Soc*. 2007, **129**, 4620−4632.

48 H. Feng, R. Cheng, X. Zhao, X. Duan and J. Li, *Nat. Commun*., 2013, **4,** 1539–1546.

49 N. A. Kumar, H. J. Choi, Y. R. Shin, D. W. Chang, L. Dai and J. B. Baek, *ACS Nano*, 2012, **6**, 1715–1723.

50 T. A. Enache, A. M. Oliveira-Brett, *Bioelectrochemistry*, 2011, **81**, 46–52.

51 J-M. You, D. Kim, S. K. Kim, M-S. Kim, H.S. Han and S. Jeon, *Sensor. Actuat. B-Chem*., 2013, **178**, 450–457.

52 A. J. Bard and L. R. Faulkner, Electrochemical Methods: *Fundamentals and Applications, Second Edition*, New York, *Wiley*, 2001.

53 J. R. Lakowicz, *Principles of Fluorescence Spectroscopy*; 3rd ed.; *Springer*: New York, 2006, pp, 282-284.

54 A. S. Al-Kady, M. Gaber, M. M. Hussein and El-Zeiny M. Ebeid, *Spectrochim. Acta. A*, 2011, **83**, 398– 405.

55 H. Chakraborti, K. Bramhaiah, N. S. John and S. K. Pal, *Phys. Chem. Chem. Phys*., 2013, **15**, 19932–19938.

56 X. Wang, S. Zhong, Y. He and G. Song, *Anal. Methods*, 2012, **4**, 360–362.

57 A. Rana and P. K. Panda, *RSC Adv.*, 2012, **2**, 12164–12168.

58 X. Shi, H. Chang, S. Chen, C. Lai, A. Khademhosseini and H. Wu, *Adv. Funct. Mater*., 2012, **22**, 751–759.

SCHEME LEGENDS

Scheme 1 Schematic diagram of *rGO/α-CD* hybrid based *Met* sensor

FIGURE LEGENDS

Figure 1 FT-IR spectra (**A**) and TGA curves (**B**) of GO, rGO, *α*-CD and *rGO/α-CD*

Figure 2 Cyclic voltammograms in the absence (background), and in the presence of 2.0×10^{-3} M *Met* at *rGO/α-CD/GCE* and at bare GCE (inset) (**A**) Cyclic voltammograms in the anodic range for the different scan rate (v); the inset shows the linear graph between the anodic peak currents (I_{pa}) and the squre root of scan rate ($v^{1/2}$) (**B**) in 0.10 M A-PBS at pH 7.40.

Figure 3 The chronoamperograms for increasing concentration of *Met* at *rGO/α-CD/GCE* in a continuously stirred solution between 0.00 and 1.46 V; The inset shows the linear graph between *Met* concentrations and the obtained amperometric responses.

Figure 4 Fluorescence spectra changes of luminol (2.0×10^{-7} M) solution after the addition of the indicated amounts of *rGO/α-CD* (**A**) The inverted and classical (the inset) Stern−Volmer plots of fluorescent intensity ratios vs [*rGO/α-CD*] (**B**) All samples were prepared with 0.10 M A-PBS at pH 7.40, and the excitation and emission wavelengths were 300 and 427 nm, respectively. The added amounts of *rGO/α-CD* are 0.0, 33, 83, 166, 250, 333, 416, 500 μg mL^{-1}, respectively.

Figure 5 Fluorescence spectra of luminol after incubation with *rGO/α-CD* and then mixed with the different amount of *Met* **(A)** The linear relationship between the fluorescence intensity and the concentration of *Met* in the concentration range from 0.0 to 1.0×10^{-2} M **(B)**. The buffer solution was 0.10 M A-PBS at pH 7.40, and the excitation and emission wavelengths were 300 and 427 nm, respectively (The added concentrations of *Met* are 0.0, 1.67, 3.33, 4.17, 5.00, 6.67, 8.33, 10.0×10^{-3} M, respectively)

Figure 6 Overall structures of *α*-CD in complexes with GO (**A**) and rGO (**B**) structures represented as stick models.

Figure 7 Side view stick model (**A, B**) and top view space filling-stick (hybrid) model (**C, D**) of schematic drawing for the *rGO/α-CD* complex with luminol and *Met*, respectively.

Scheme 1

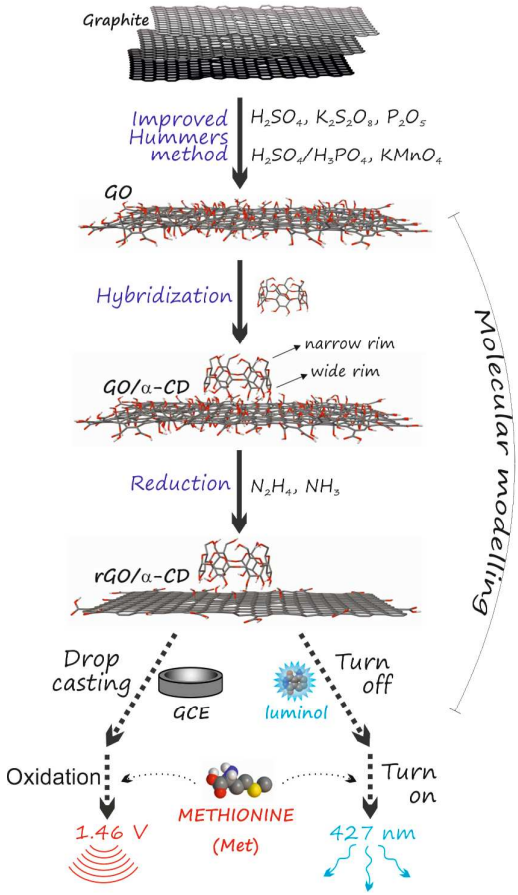

Figure 1

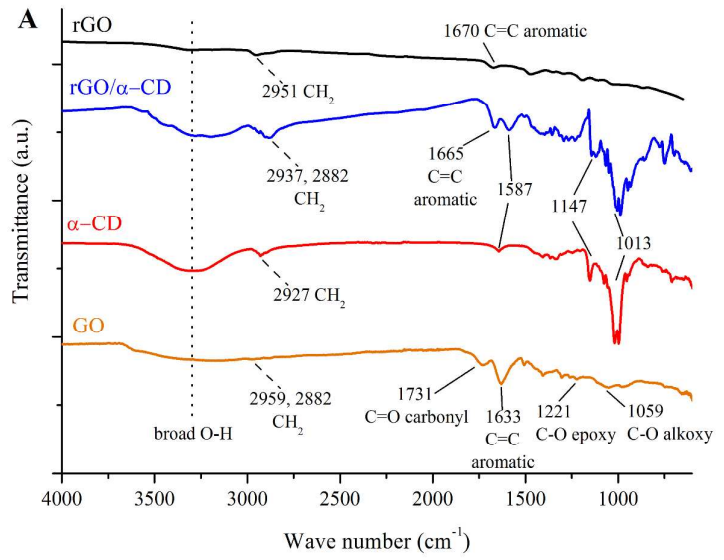

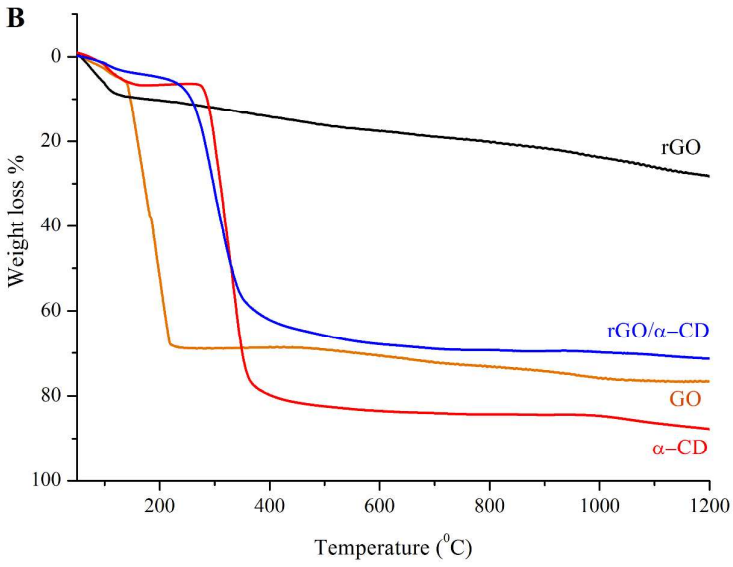

Figure 2

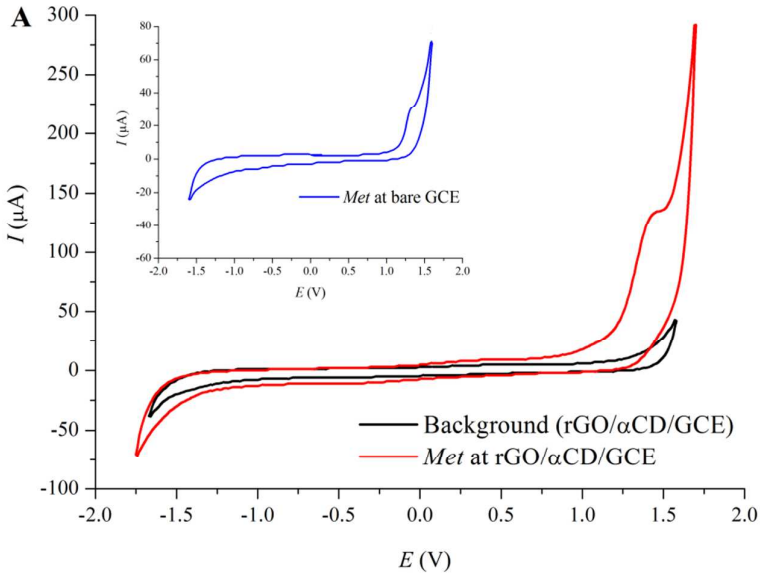

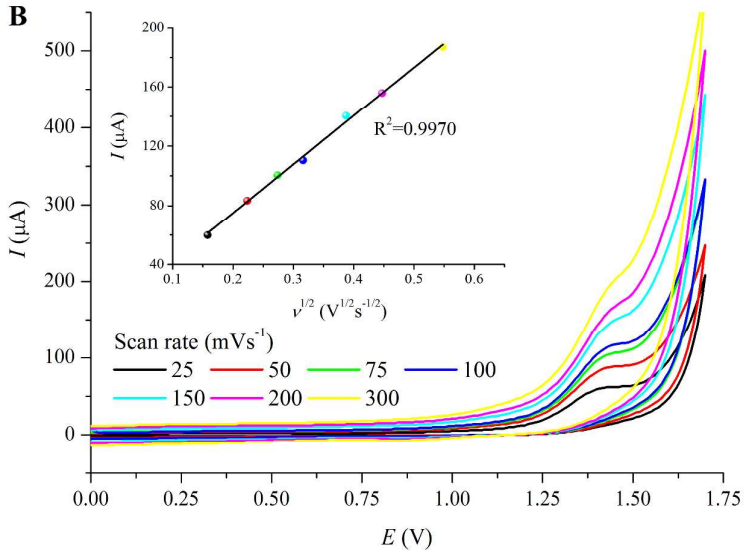

Figure 3

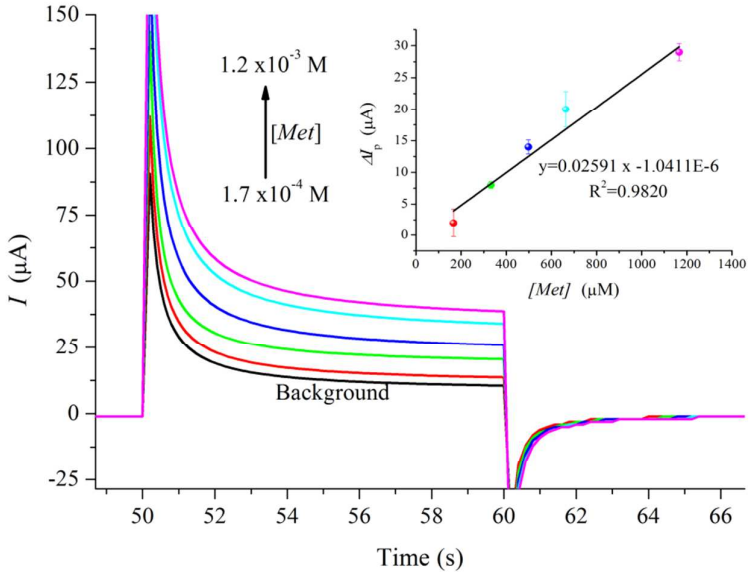

Figure 4

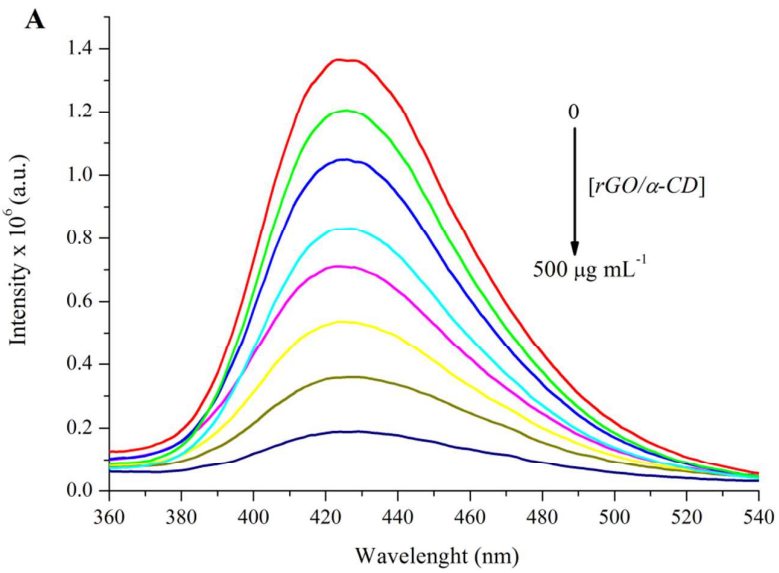

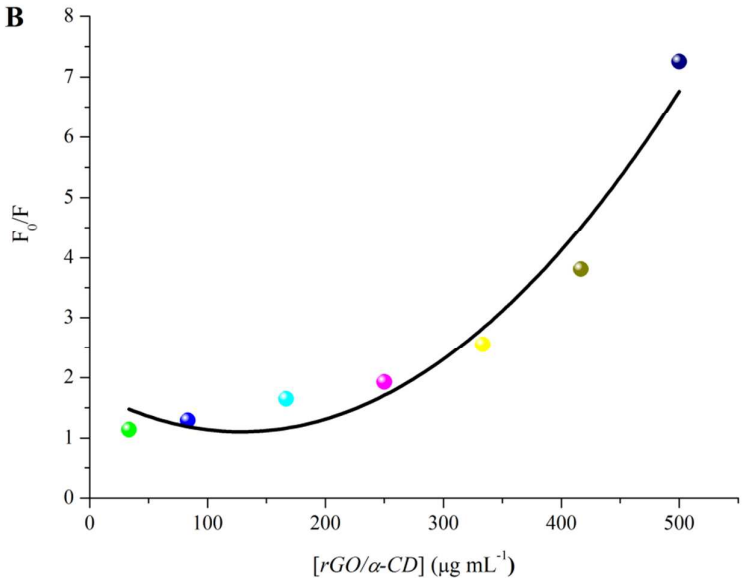

Figure 5

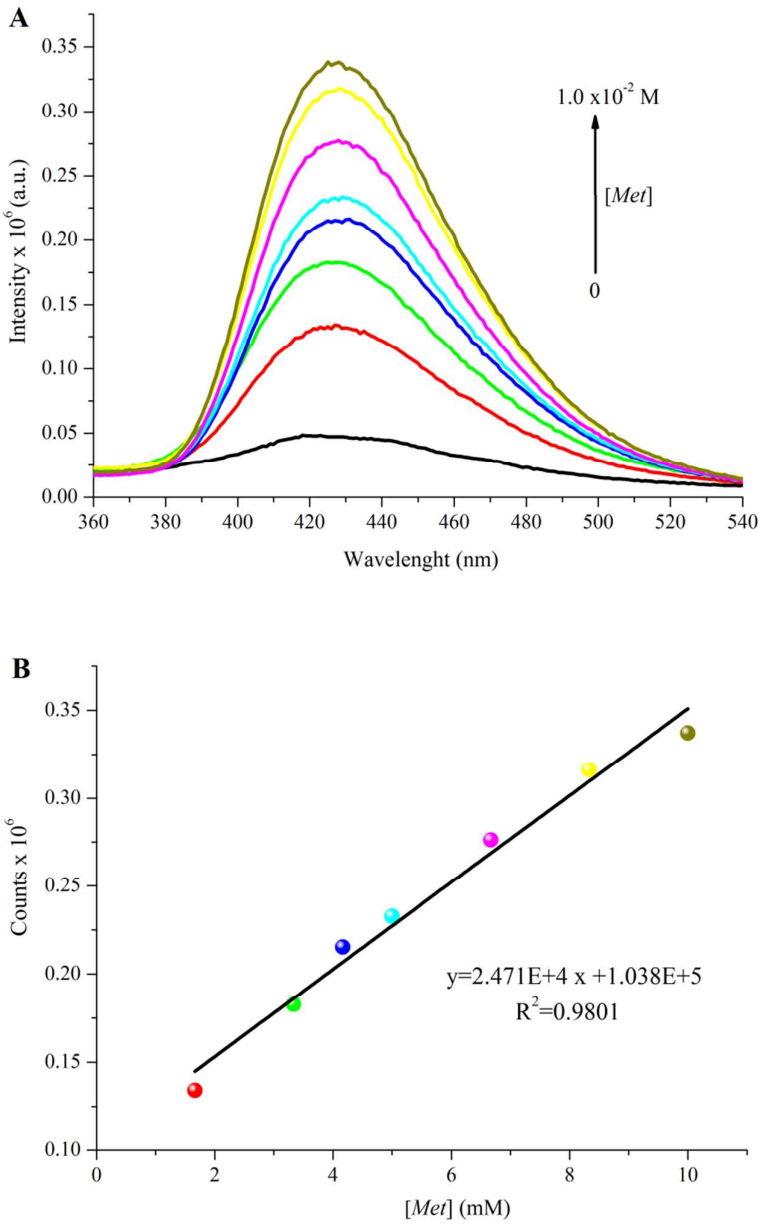

Figure 6

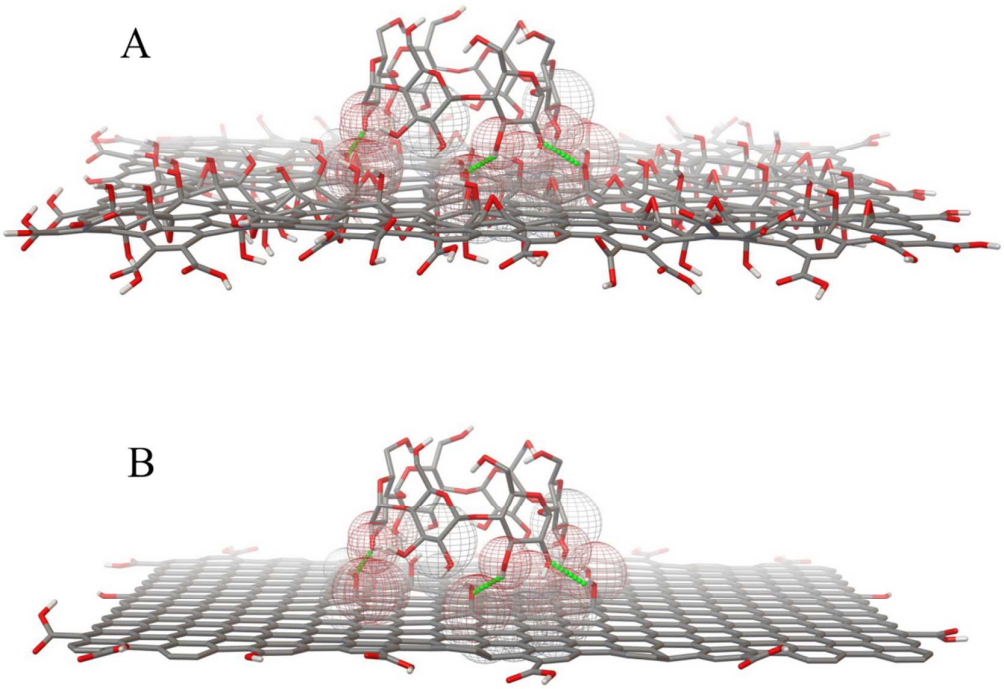

Figure 7